Phase diagrams of block copolymer melts by dissipative particle dynamics simulations

ARTICLE *in* THE JOURNAL OF CHEMICAL PHYSICS · DECEMBER 2013

Impact Factor: 2.95 · DOI: 10.1063/1.4837215 · Source: PubMed

3 AUTHORS, INCLUDING:

Yaroslav V Kudryavtsev
Russian Academy of Sciences
62 PUBLICATIONS **353** CITATIONS

SEE PROFILE

Phase diagrams of block copolymer melts by dissipative particle dynamics simulations

Alexey A. Gavrilov, Yaroslav V. Kudryavtsev, and Alexander V. Chertovich

Citation: The Journal of Chemical Physics **139**, 224901 (2013); doi: 10.1063/1.4837215
View online: http://dx.doi.org/10.1063/1.4837215
View Table of Contents: http://scitation.aip.org/content/aip/journal/jcp/139/22?ver=pdfcov
Published by the AIP Publishing

Phase diagrams of block copolymer melts by dissipative particle dynamics simulations

Alexey A. Gavrilov,[1,2,a)] Yaroslav V. Kudryavtsev,[3] and Alexander V. Chertovich[1]
[1]*Physics Department, Lomonosov Moscow State University, Leninskie gory, 1, build. 2, 119991 Moscow, Russia*
[2]*Institute for Advanced Energy Related Nanomaterials, University of Ulm, Albert-Einstein-Allee 47 Ulm, D-89069, Germany*
[3]*Topchiev Institute of Petrochemical Synthesis, Russian Academy of Sciences, Leninsky prosp. 29, 119991 Moscow, Russia*

(Received 23 August 2013; accepted 15 November 2013; published online 10 December 2013)

Phase diagrams for monodisperse and polydisperse diblock copolymer melts and a random multiblock copolymer melt are constructed using dissipative particle dynamics simulations. A thorough visual analysis and calculation of the static structure factor in several hundreds of points at each of the diagrams prove the ability of mesoscopic molecular dynamics to predict the phase behavior of polymer systems as effectively as the self-consistent field-theory and Monte Carlo simulations do. It is demonstrated that the order-disorder transition (ODT) curve for monodisperse diblocks can be precisely located by a spike in the dependence of the mean square pressure fluctuation on χN, where χ is the Flory-Huggins parameter and N is the chain length. For two other copolymer types, the continuous ODTs are observed. Large polydispersity of both blocks obeying the Flory distribution in length does not shift the ODT curve but considerably narrows the domains of the cylindrical and lamellar phases partially replacing them with the wormlike micelle and perforated lamellar phases, respectively. Instead of the pure 3d-bicontinuous phase in monodisperse diblocks, which could be identified as the gyroid, a coexistence of the 3d phase and cylindrical micelles is detected in polydisperse diblocks. The lamellar domain spacing D in monodisperse diblocks follows the strong-segregation theory prediction, $D/N^{1/2} \sim (\chi N)^{1/6}$, whereas in polydisperse diblocks it is almost independent of χN at $\chi N < 100$. Completely random multiblock copolymers cannot form ordered microstructures other than lamellas at any composition. © *2013 AIP Publishing LLC*. [http://dx.doi.org/10.1063/1.4837215]

I. INTRODUCTION

For decades, self-assembling in block copolymer systems remains a field where topics for basic research and opportunities for practical applications only grow with developing novel synthetic routes and advanced techniques for studying the stunning diversity of observable microstructures.[1–4] All the time, field-based methods, particularly the self-consistent field theory (SCFT),[5,6] dominated in the theoretical studies of phase behavior. Particle-based approaches utilizing various versions of coarse-grained Monte Carlo and molecular dynamics simulation techniques were involved as an important yet auxiliary tool, which enabled detecting the phases that are in principle available for a particular system and roughly characterizing their morphology and phase transitions.[7,8] Finite size effects and time restrictions in modeled systems were the main factors that prevented researchers from considering the results of coarse-grained simulations as the full value data.

Advances in computing facilities, as well as practical needs for studying many specific polymer systems on a quantitative level, led to the formulation of a multiscale modeling paradigm,[9] which considers field-based and particle-based methods as complementary approaches that should benefit from each other. In the field of block copolymers, this general tendency stimulated two lines of research. First of them implies developing hybrid techniques[10–13] that involve the concept of a self-consistent field into the calculation of interactions in the ensemble of particles. In that way, the evaluation of interchain interactions becomes a considerably less time-consuming procedure. The second line, to which the present investigation belongs, focuses on further developing various pure particle-based approaches[14–22] in order to overcome computational restrictions by adjusting the level of coarse-graining, using multiprocessor platforms and parallel programming codes.

Dissipative particle dynamics (DPD) is a well-established mesoscopic dynamics method[23,24] utilizing the bead – spring model of a polymer fluid. It was used for studying the general features of microstructure formation in diblock,[25–29] triblock,[30,31] multiblock,[32–34] multiarm,[35] and cyclic[36] copolymers, as well as for visualizing expectable morphologies for several specific diblock[37–41] and multiblock[42] copolymer systems. These are only a few of many recent references to DPD applications, not to mention studies in which block copolymers were confined in thin films or adsorbed at liquid/liquid and liquid/solid interfaces or subjected to cross-linking and other chemical transformations.

a)Author to whom correspondence should be addressed. Electronic mail: gavrilov@polly.phys.msu.ru

In spite of its growing popularity, DPD is up to now a mainly qualitative approach with prevailing visual comparison of its results to experimental data. In part, it can be explained by absence of an internal scale associated with the particles[43] and rather complex procedure of mapping its parameters onto observable quantities.[24] Another possible reason could be related to the lack of benchmarking data on simple model systems comparing DPD with other methods.

The first purpose of the present study is to provide such data by constructing the DPD phase diagram for a monodisperse AB diblock copolymer melt, which can be compared to the current SCFT,[44] Monte Carlo,[19] and previous DPD[26–28] phase diagrams for the same system. To this end, an unprecedented volume of parallel computations on the modern cluster is performed.

In recent years, growing attention has been paid to the role of block polydispersity in self-assembling of copolymers,[45] which becomes a convenient tool for controlling their morphology and domain characteristics. Though the DPD technique was applied to simulate the effects of polydispersity on the *in situ* block copolymer formation and ordering,[46,47] only recently it was first used to study the simplest model of a premade diblock copolymer melt with one polydisperse block.[48] In this work, the situation when both blocks are polydisperse and their lengths are described by the most probable (Flory) distribution is considered. The DPD phase diagram is presented and compared to that of the same monodisperse melt, as well as to the diagrams obtained for the polydisperse AB diblock copolymer melts using SCFT[49] and Monte Carlo simulations.[20]

The last diagram in the present paper summarizes our DPD study of microphase separation in random multiblock copolymers of different compositions. Recently[34] we reported on the possibility of forming an imperfect lamellar microstructure in the symmetric AB random copolymer melt under strong[50] and superstrong[51] segregation conditions. In this study, our considerations are extended to compositionally asymmetric multiblocks in order to find whether any microstructure other than lamellas is possible. Knowledge of expected morphologies can be very useful for all who want to use DPD simulations for predicting self-assembling properties of real diblock copolymer melts.

II. SIMULATION TECHNIQUE AND MODELS

Simulations were performed using the DPD-VV integration scheme[52] that implements the modified velocity-Verlet algorithm[53] for solving Newton's equations of motion for interacting particles,

$$\frac{d\mathbf{r}_i}{dt} = \mathbf{v}_i, \quad m_i \frac{d\mathbf{v}_i}{dt} = \mathbf{F}_i. \tag{1}$$

Here $\mathbf{r}_i$, $\mathbf{v}_i$, and m_i denote the radius vector, velocity, and mass of an ith particle. Let the force $\mathbf{F}_i$ acting on it be written as a sum of pairwise additive contributions,

$$\mathbf{F}_i = \sum_{j \neq i} \left(\mathbf{F}^{\mathrm{C}}_{ij} + \mathbf{F}^{\mathrm{D}}_{ij} + \mathbf{F}^{\mathrm{R}}_{ij} \right), \tag{2}$$

where the summation is performed over all other particles within a certain cutoff radius r_c. We assume that all quantities in Eqs. (1) and (2) are dimensionless and for simplicity set all m_i and r_c to unity.

The conservative force $\mathbf{F}^{\mathrm{C}}_{ij}$ includes a soft core repulsion force $\mathbf{f}^{nb}_{ij}$ between non-bonded contacting particles and a bond elasticity force $\mathbf{f}^{b}_{ij}$ in bead-spring polymer chains,

$$\mathbf{F}^{\mathrm{C}}_{ij} = \mathbf{f}^{nb}_{ij} + \mathbf{f}^{b}_{ij}, \tag{3}$$

$$\mathbf{f}^{nb}_{ij} = \begin{cases} a_{ij}(1 - r_{ij})\bar{\mathbf{r}}_{ij}, & r_{ij} < 1 \\ 0, & r_{ij} \geq 1, \end{cases} \qquad \mathbf{f}^{b}_{ij} = -K_{ij}\mathbf{r}_{ij}, \tag{4}$$

where $\mathbf{r}_{ij} = \mathbf{r}_i - \mathbf{r}_j$, $r_{ij} = |\mathbf{r}_{ij}|$, $\bar{\mathbf{r}}_{ij} = \mathbf{r}_{ij}/r_{ij}$, and a_{ij} is a maximum repulsion between particles i and j attained at $\mathbf{r}_i = \mathbf{r}_j$, K_{ij} is a spring constant (we take $K_{ij} = 4$ for neighboring particles in a chain, as proposed in Ref. 24, and zero for others).

Other constituents of $\mathbf{F}_i$ are a dissipative force $\mathbf{F}^{\mathrm{D}}_{ij}$ (friction) and a random force $\mathbf{F}^{\mathrm{R}}_{ij}$,

$$\mathbf{F}^{\mathrm{D}}_{ij} = -\frac{\sigma^2}{2k_{\mathrm{B}}T}[\omega(r_{ij})]^2(\mathbf{v}_{ij} \cdot \bar{\mathbf{r}}_{ij})\bar{\mathbf{r}}_{ij},$$
$$\mathbf{F}^{\mathrm{R}}_{ij} = \sigma\omega(r_{ij})\frac{\zeta}{\sqrt{\delta t}}\bar{\mathbf{r}}_{ij}, \qquad \omega(r) = \begin{cases} 1 - r, & r \leq 1 \\ 0, & r > 1 \end{cases}, \tag{5}$$

where σ is a noise amplitude, k_{B} is the Boltzmann constant, T is temperature, $\mathbf{v}_{ij} = \mathbf{v}_i - \mathbf{v}_j$, ζ is a normally distributed random variable with zero mean and unit variance chosen independently for each pair of particles, and δt is a time step. We take that $k_{\mathrm{B}}T = 1$ and introduce a dimensionless time unit as

$$\tau = r_c\sqrt{\frac{m}{k_{\mathrm{B}}T}} = 1. \tag{6}$$

The Groot-Warren thermostat defined by Eq. (5), where the random and dissipative forces serve as a heat source and sink, respectively, preserves momentum for each pair of interacting particles. Following Ref. 24 we choose the noise parameter σ and the reduced particle density ρ_0 both equal to 3 that provides an optimal balance between fast thermal relaxation and stability of the equilibrium state. In the same paper it was shown that for $\rho_0 = 3$ one should take a_{ij} for similar particles equal to 25 in order to get a reasonable compressibility of the DPD liquid, while the repulsion parameter for dissimilar particles could be related to the Flory-Huggins interaction parameter χ as follows:

$$a_{ij} = \chi/0.306 + 25, \quad i \neq j. \tag{7}$$

The time step for integrating Eq. (1), $\delta t = 0.04$, was chosen according to Ref. 24. A *simulation box* of sizes $l_x \times l_y \times l_z = 32 \times 32 \times 32$ containing 98 304 ($\sim 10^5$) particles was used, if otherwise is not specified. The periodic boundary conditions were imposed in all three directions.

Three types of AB copolymer melts were modeled in this study: monodisperse diblock copolymer (below referred to as m-diblock) with chains of the fixed length $N = 16$, polydisperse diblock copolymer (random or r-diblock), and completely random multiblock copolymer (r-multiblock) with

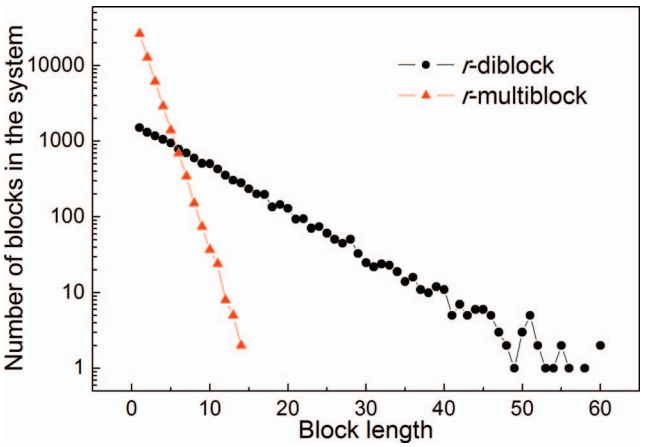

FIG. 1. Block length distributions in the symmetric ($f = 0.5$) *r*-diblock and *r*-multiblock.

chains containing in average 16 and 32 units, respectively. *R*-diblock and *r*-multiblock were characterized by an exponential (Flory) distribution of chain lengths and A and B block lengths. Copolymer composition, which is described by the molar fraction of A units, f, was varied in a wide interval $0.125 \le f \le 0.5$.

Any copolymer of a prescribed composition was synthesized from a set of non-connected identical DPD particles. Chain-growth polymerization and monomer "coloring" were used to obtain the desired chain length distributions and monomer sequences. In the case of *m*-diblocks, growth of any chain was terminated as soon as its polymerization degree reached the value of 16; at full conversion a given part of each chain (from 2 to 8 units) was designated as an A block to get a desired composition. *R*-diblocks were obtained in a different way. First of all, DPD particles were marked as A and B monomers according to a prescribed value of the parameter f. Then they were polymerized by allowing bond formation between similar units only, until the number average lengths of A and B oligomers attain $16f$ and $16(1-f)$, respectively. The obtained system was converted into AB copolymer melt of *r*-diblock type by random coupling of dissimilar oligomer pairs. *R*-multiblocks were synthesized as follows. Identical DPD particles were randomly polymerized until the number average polymerization degree in the system, $\bar{N}$, attained the value of 32, then monomer units of all chains were marked as A or B units with the probabilities f and $1-f$, respectively. As is seen from Figure 1, the block length distributions in the symmetric (equimolar) *r*-diblock and *r*-multiblock indeed have an exponential type.

The number average block lengths for an infinite *r*-multiblock chain are $\bar{N}_{A\infty} = (1-f)^{-1}$, $\bar{N}_{B\infty} = f^{-1}$. If the infinite macromolecule is randomly cut into chains containing in average $\bar{N}$ units, the average block lengths are decreased. Considering changes in the block length distributions and retaining only the terms linear in $1/\bar{N}$ we easily find for $\bar{N} \gg 1$,

$$\begin{aligned} \bar{N}_A &= \frac{1}{1-f}\left(1 - \frac{f}{\bar{N}(1-f)} + O\left(\frac{1}{\bar{N}^2}\right)\right), \\ \bar{N}_B &= \frac{1}{f}\left(1 - \frac{1-f}{\bar{N}f} + O\left(\frac{1}{\bar{N}^2}\right)\right), \end{aligned} \tag{8}$$

so that a virtual constituting diblock, which is obtained by cutting all blocks of a multiblock in half, has the length

$$N_c = \frac{\bar{N}_A + \bar{N}_B}{2} \approx \frac{1}{2f(1-f)} - \frac{f^3 + (1-f)^3}{2\bar{N}f^2(1-f)^2}. \tag{9}$$

Since simulated chains are rather short, fluctuations can play an important role in the model system behavior. They are controlled by a Ginsburg parameter, also known as the invariant degree of polymerization[25] $N_{inv} = b^6 v^{-2} \bar{N} = 6^3 (R_g^3 \rho_0 / \bar{N})^2$, where b, v, and R_g are the statistical segment size and volume and the gyration radius of a chain, respectively. Our simulations for an athermal melt of *m*-diblocks at $\rho_0 = 3$ yield $R_g^2 = 2.6$ (for strictly Gaussian chains with $b = 1$ there should be $R_g^2 = 16/6 \approx 2.67$, which is rather close) so that $N_{inv} = 133$, which is of the same order as in a typical Monte Carlo study.[54]

In the course of copolymer synthesis, the interaction parameter a_{ij} was set to 25 for all particle pairs, which corresponds to an athermal melt with $\chi = 0$. Therefore, in the initial state all copolymer melts were characterized by a random distribution of chains in the simulation box. Then, the value of χ was instantaneously increased and the system was relaxed for 2×10^8 time steps in the case of *r*-diblocks and for 3×10^7 time steps in two other cases. The final states form a regular grid in the domain $\chi_{min} \le \chi \le \chi_{max}$ (*m*-diblock: $\chi_{min} = 0$, $\chi_{max} = 7.65$, 64 points; *r*-diblock: $\chi_{min} = 0$, $\chi_{max} = 7.65$, 32 points; *r*-multiblock: $\chi_{min} = 18.36$, $\chi_{max} = 48.96$, 64 points), $0.125 \le f \le 0.5$ (7 points in all the cases) that enables one to construct a phase diagram in the standard $\chi N - f$ coordinates. Such diagram contains 448 figurative points for *m*-diblocks and *r*-multiblocks and 224 points for *r*-diblocks, which is much more than reported in the literature for any simulation technique.[19,20,26–28,36] All simulations were performed at Lomonosov Moscow State University Supercomputer facilities.

III. STRUCTURE ANALYSIS

After relaxation, the final morphology at each point was thoroughly analyzed by calculating the static structure factor and checking the positions of the satellite peaks, as well as by viewing 3D representations of the simulation box from different angles. Static structure factor is proportional to the intensity of a scattered beam measured in light, X-ray, electron or neutron elastic scattering experiments,

$$S(q) = \frac{1}{n}\left\langle \left| \sum_{j=1}^{n} exp(i\boldsymbol{q}\boldsymbol{r}_j) \right|^2 \right\rangle, \tag{10}$$

where n is the total number of particles and averaging is performed over the wave vector set $\{q_x, q_y, q_z\} = \{2\pi k/l_x, 2\pi m/l_y, 2\pi p/l_z\}$, where k, m, p are integers from 1 to 32, and over a sequence of independent system conformations. As a rule, 50 conformations separated by 10 000 DPD steps were taken for the averaging. Six types of ordered microstructures that were observed in simulations are shown in Figure 2.

Analyzing the q-dependence of the structure factor one can detect a long-range (presence of satellite peaks) or short-range ordering, estimate the characteristic size of domains

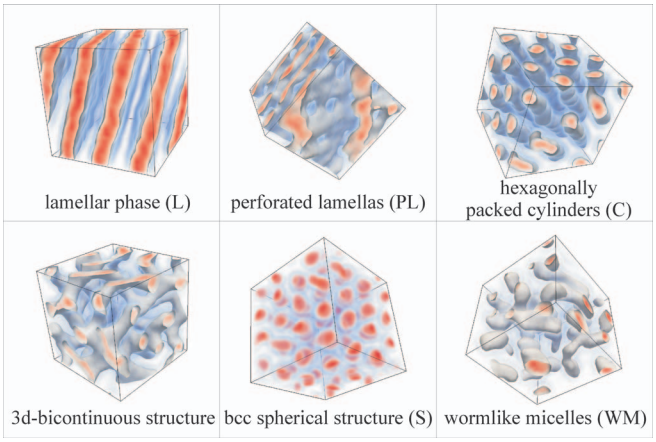

FIG. 2. Typical snapshots of the observed microstructures. In order to obtain field-based representations of the structures, the simulation box was divided into cells of unit volume, the number density was calculated in each of these cells and plotted on a color scale.

(main peak position) and its dispersion (peak width at half-height).

The structure factors for ordinary and perforated lamellas (L and PL) are shown in Figure 3. $S(q)$ dependence for the PL microstructure contains additional peaks at $\sqrt{3}$, $\sqrt{7}$, $\sqrt{11}$, which are presumably related to a hexagonal ordering of perforations. Though PL is considered as a metastable structure in the framework of SCFT,[55] it is often observed in laboratory and numerical experiments, which fact is attributed either to idealizations of the theoretical model, such as assuming infinite molecular mass and neglecting fluctuations, or just to the small difference between energies of PL and concurrent bicontinuous structures.

Figure 4 demonstrates typical structure factors with the peak sets characteristic of cylindrical (C) and spherical (S) micelles ordered in hex and bcc morphologies, respectively. Whereas cylinders are almost as well studied as lamellas, the S microstructure in copolymers is rather common only in experimental systems, where it can be obtained either by order-disorder transition (ODT)[56] or order-order transition (OOT).[57] Its identification by SCFT,[13] in Monte Carlo[19,20] and even DPD[25,41] simulations is usually difficult, if not impossible because of the long equilibration time.

Figure 5 reports on the least ordered structures with ill-defined peaks on the $S(q)$ dependence. The top picture corresponds to a 3d-bicontinuous microstructure, which could be provisionally identified as the gyroid (G) phase, as it contains five of first seven peaks (those at $14^{1/2}$ and $20^{1/2}$ are missing). The bottom plot describes the structure without long-range order, which we visually associate with wormlike micelles (WM).

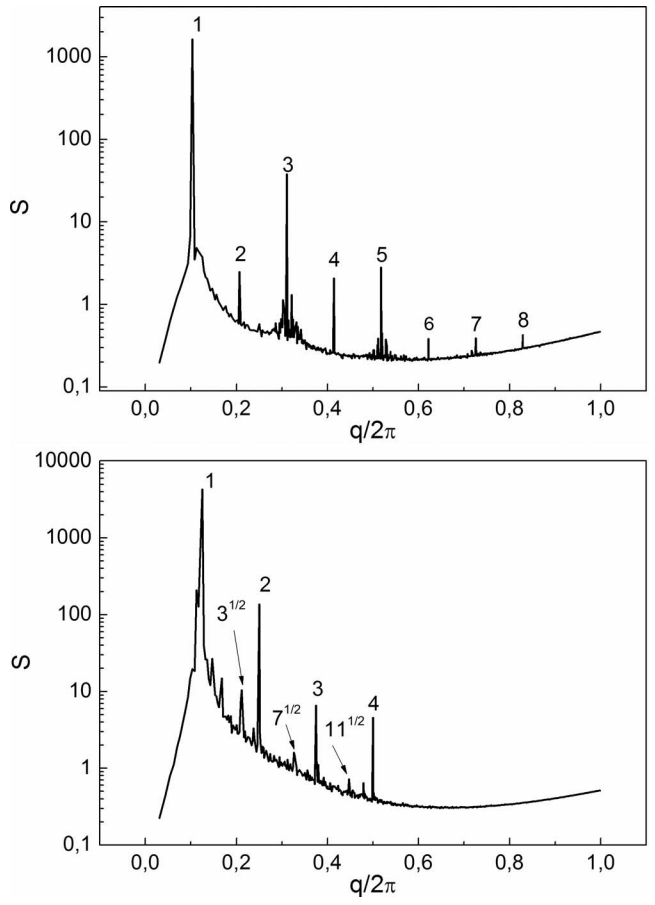

FIG. 3. Typical static structure factors for the (top) L and (bottom) PL microstructures in m-diblocks. Square-root peaks in the bottom figure could belong to a hex microstructure formed by perforations. Number of integer peaks for the L structure is twice as many as that for the PL one because of a higher χN value in the former case.

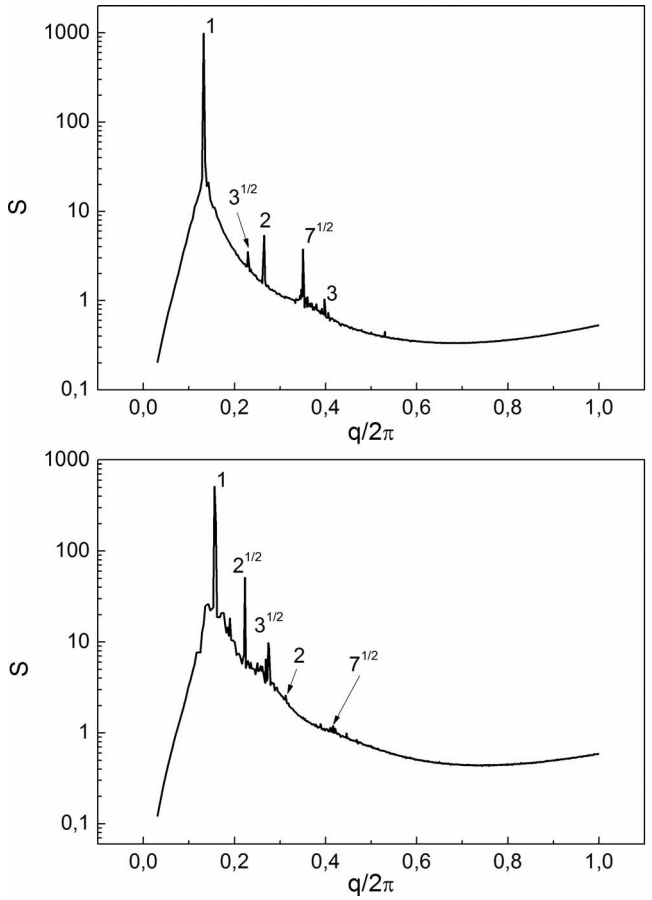

FIG. 4. Typical static structure factors for the (top) C and (bottom) S microstructures in m-diblocks. Though the peak sets are nearly identical, cylinders and spheres can be easily distinguished visually.

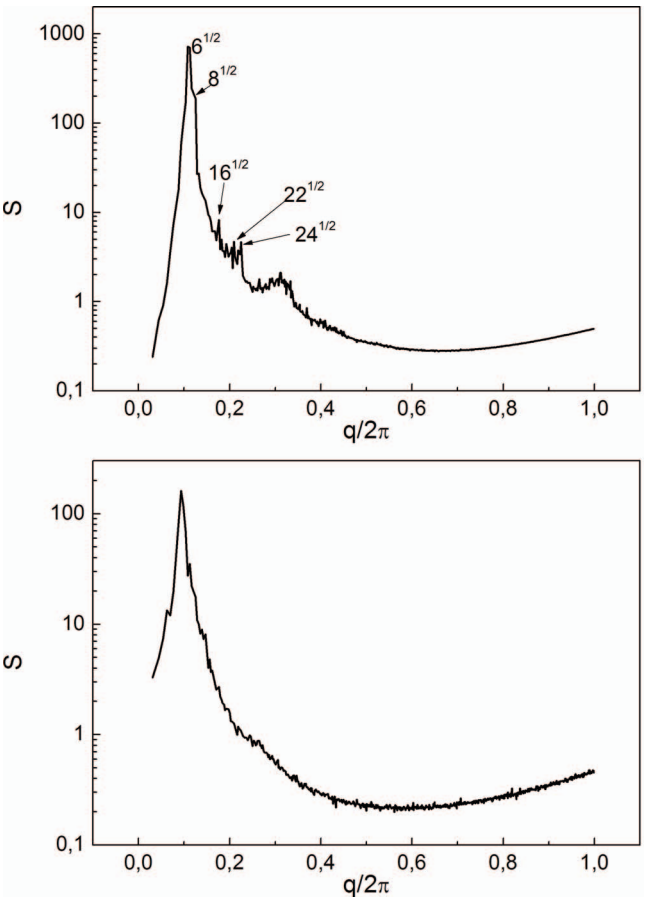

FIG. 5. Typical static structure factors for the (top) 3d-bicontinuous structure in *m*-diblocks and (bottom) wormlike micelles in *r*-diblocks.

IV. PHASE DIAGRAMS

A. Monodisperse diblocks

The phase diagram for *m*-diblocks is plotted in Figure 6. With 448 figurative points (64 points for each of 7 chosen compositions) for the chains of $N = 16$ units, it can be considered as a much more accurate version of the first DPD phase diagram[26] based on the calculations of Groot and Madden[25] for 27 model *m*-diblocks of $N = 4$ and 10 units. The following DPD studies[27,28] were focused, respectively, on testing an alternative (Lowe-Andersen) thermostat and securing the gyroid phase via adjusting sizes of the simulation box rather than on mapping an entire phase diagram for *m*-diblocks.

The lowest curve in Figure 6 separates the disordered (D) phase from all others thus marking the ODT at a given copolymer composition. It can be located either visually or by appearance of a pronounced main maximum on the $S(q)$ dependence. Order of the phase transition can be determined by introducing the instantaneous pressure[53] using the Clausius virial theorem

$$p_{\alpha\beta} = \frac{1}{V}\sum_i m_i v_{i\alpha} v_{i\beta} + \frac{1}{V}\sum_i \sum_{j>i} F^{\mathrm{C}}_{i\alpha} r_{ij\beta}, \qquad (11)$$

which reduces to the scalar (hydrodynamic) pressure $p = \mathrm{Tr}(p_{\alpha\beta})/3$ for isotropic systems. By averaging over subsequent system configurations, one finds the mean scalar pressure

$$\bar{p} = \rho k_{\mathrm{B}} T + \frac{1}{3V}\left\langle \sum_i \sum_{j>i} \mathbf{F}^{\mathrm{C}}_i \mathbf{r}_{ij} \right\rangle, \qquad (12)$$

and the mean square fluctuation (variance) $\delta p^2 = \overline{p^2} - \bar{p}^2$. Simulations demonstrate that the dependence of δp^2 on χN for any fixed *m*-diblock composition exhibits a steep increase (Figure 7, top row) indicating about the first order (discontinuous) transition. Note that in the ordered state pressure fluctuations are markedly non-monotonous with χN for the symmetric copolymer forming lamellas and are weakly decreasing for the strongly asymmetric *m*-diblock forming spherical micelles. The dependence of the variance of the internal energy (which is proportional to the heat capacity of the system) on χN was also calculated in order to check these conclusions. Behavior of the corresponding curves plotted in the bottom row of Figure 7 is similar to that of the pressure variance.

In order to check consistency of the results based on pressure measurements, eigenvalues of the pressure tensor given Eq. (11) were calculated and found to be equal after the system is equilibrated. Another test was related to the reversibility of the ODT transition. At a given composition, a hysteresis of about $\Delta\chi N/2 \approx 2.0$ was detected, which is equal to the half vertical distance between neighboring figurative points at the phase diagram, coinciding with the precision in the ODT location.

Ordered phases (L, PL, 3d, C, and S) and their succession in Figure 6 are typical for the experimental *m*-diblock phase diagrams.[2] Phase domains are separated with curves marking OOTs of continuous type, which do not directly affect pressure and other measurable characteristics. However, sometimes after detecting a new phase an old one was again detected in a few points corresponding to higher χN, probably because of small energy difference between the two phases in the transition vicinity. To overcome this difficulty in a consistent manner, we assigned a point to a new phase as soon as it was unambiguously detected for the first time upon bottom-up shift in the phase diagram. Some of the OOT curves in

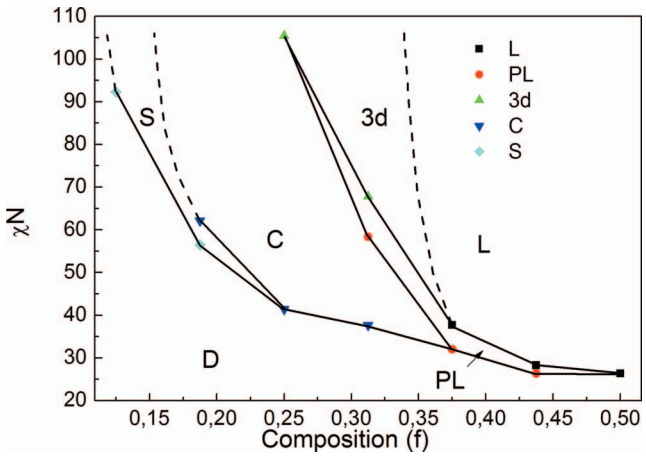

FIG. 6. DPD phase diagram for *m*-diblocks. Dashed lines display an expected behavior. Markers show the points at which the corresponding morphologies were first observed on increasing χN at fixed *f*.

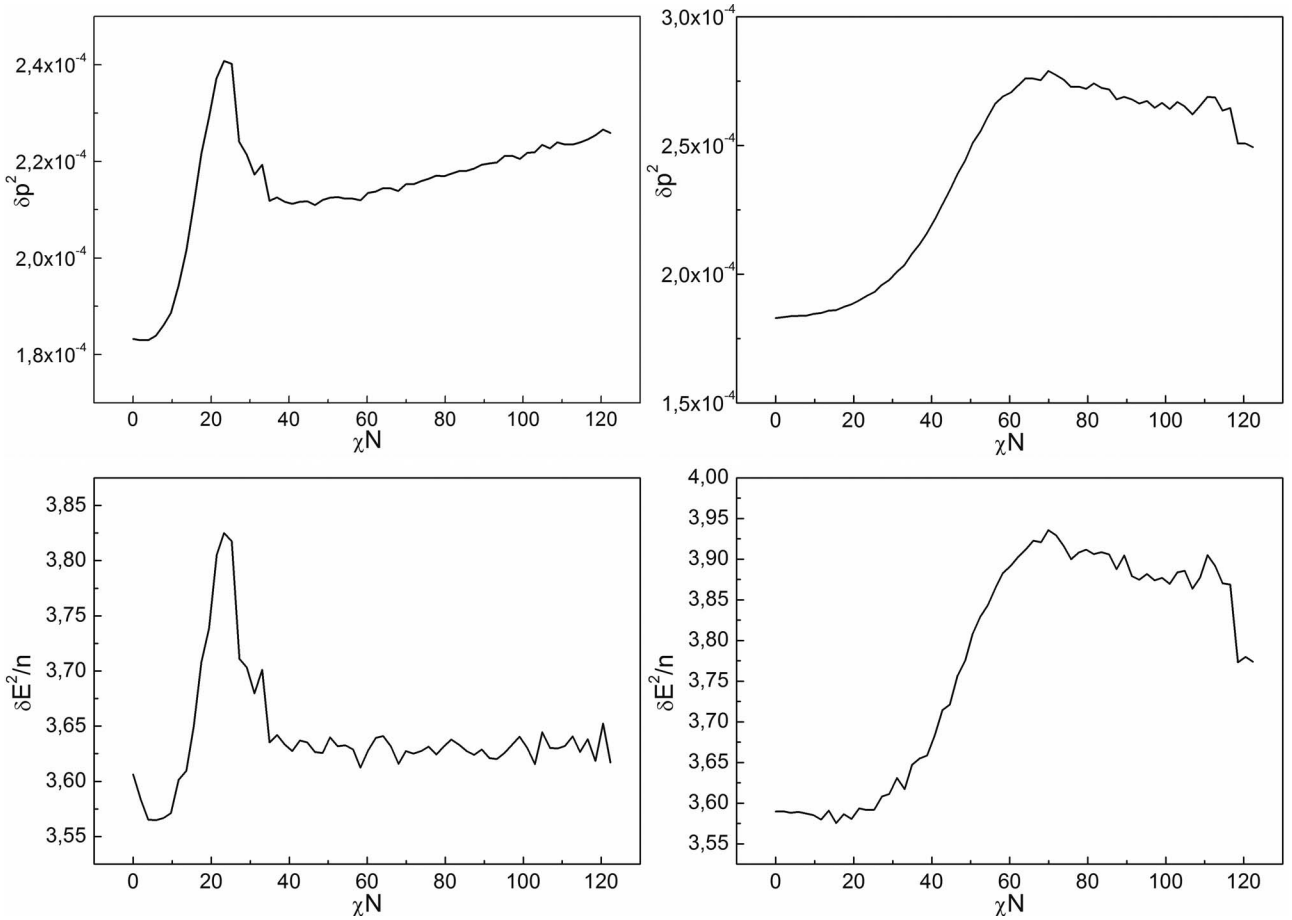

FIG. 7. Dependence of the (top row) pressure variance δp^2 and (bottom row) internal energy variance δE^2 on χN for the (left, $f = 0.5$) symmetric and (right, $f = 0.125$) strongly asymmetric m-diblocks.

Figure 6 pass through only one of the explored points so that they cannot be precisely located and therefore are drawn with dashed lines.

Comparing our result to the current version of SCFT phase diagram,[44] it is easy to see close similarity in the location of major domains, except for 3d and PL ones, which are reduced to a considerably narrower G domain in the theoretical case. It should be mentioned that we avoid identifying the 3d microstructure as G because of certain difficulties with obtaining the gyroid phase by DPD simulations, which are in detail described in Ref. 26. In fact, we obtained an evident G cell in the 23 × 23 × 23 box, which size was chosen according to the position of the main maximum $q_{\max}$ in the $S(q)$ dependence shown in Figure 5: $l = 2\pi\sqrt{6}/q_{\max} \approx 22.7$ (in Ref. 26, where the DPD model with somewhat different numerical parameters was used, a gyroid structure was also obtained in the same specific 23 × 23 × 23 box for $f = 0.35$ and $\chi N = 50$). However, our simulations in the eight time larger box 46 × 46 × 46, which was also commensurate with the preferred unit cell, resulted in the formation of a PL microstructure instead of eight G cells. That is why we decided to plot the phase diagram (Figure 6) that is based on the results for the simulation box of standard sizes 32 × 32 × 32. Visual analysis demonstrated that the obtained 3d microstructure can be considered as a mixture of gyroid and double-diamond morphologies, similarly to the AB copolymer bicontinuous microstructures simulated by DPD in the literature.[29,34,58] Also we did not make special efforts to detect the bicontinuous orthorhombic (O^{70}) phase and particulate close packed spherical (S_{cp}) phase, which are present as very small domains in the SCFT diagram[44] and got some experimental evidence.[59,60]

An obvious virtue of the DPD phase diagram is predicting the possibility of ODT from the disordered state directly to the S, C, PL, and L phases. On the contrary, random phase approximation (RPA),[61] which is a mean-field approximation of SCFT at weak segregations, claims that all transition curves meet at the critical point and the ODT curve separates D and S phases at any place of the phase diagram. This deficiency can be removed by taking into account fluctuation corrections,[62] which shift SCFT critical point to $(\chi N)_{\rm cr} = 10.5 + 41.0N_{inv}^{-1/3}$, $f_{\rm cr} = 0.5$. The last expression lacks theoretical support for chains $N_{inv} < 10^4$ and its formal application at $N_{inv} = 133$ yields $(\chi N)_{\rm cr} \approx 18.5$, which is considerably less than the critical point ordinate of 26.4 obtained in our DPD simulations. The situation is similar to the MC study of Ref. 54, where the simulated $(\chi N)_{\rm cr}$ was much higher than predicted by SCFT despite fluctuation corrections.

Many other parallels can be found by comparing the DPD and MC[19] phase diagrams for m-diblocks. Both methods predict the same major phases (L, G, C) and the first-order ODT. However, the nature of MC technique using a lattice with

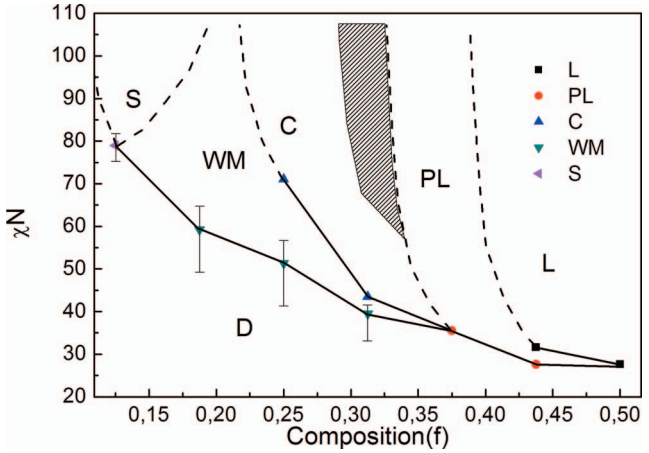

FIG. 8. DPD phase diagram for *r*-diblocks. The domain of C and 3d coexisting phases is shaded. Dashed lines display an expected behavior. Markers show the points at which the corresponding morphologies were first observed on increasing χN at fixed f.

predetermined spatial symmetry causes some problems, which are successfully avoided with DPD. For instance, MC predicts vertical OOT curves, which are not confirmed experimentally, and cannot detect spherical morphologies in monodisperse diblocks, which are readily formed in systems with strong a compositional asymmetry. On its bright side, MC usually provides well-resolved structure factor peaks for C, S, and L phases, which, once again, should be attributed to its lattice nature.

B. Random diblocks

The phase diagram for *r*-diblocks (both A and B blocks are polydisperse with $PDI_A = PDI_B \approx 2$) is plotted in Figure 8. In comparison to *m*-diblocks (Figure 6), the L domain is narrower giving more space to perforated lamellas. Pure 3d phase is absent but it coexists with the C phase. The biphasic domain is shaded because such morphology could correspond to a frozen rather than equilibrium state due to high χN values. The C domain is considerably narrower than in Figure 6, neighboring wormlike micelles on its left, a phase with rather high segregation of A and B units yet revealing no long-range order.

The ODT curve is slightly shifted up, with the critical point at $(\chi N)_{cr} \approx 27.6$, $f_{cr} = 0.5$ so that the difference with the monodisperse case lies within the error range. The latter fact contradicts theoretical considerations, which predict a nearly twofold decrease in $(\chi N)_{cr}$ either in the mean field approximation (RPA)[63,64] or with account for the fluctuation corrections.[65] However, it is known that for the diblocks with only one polydisperse block similar SCFT predictions about lowering the critical point and the ODT curve in general[66–68] clearly disagree with the experimental,[69] MC,[20,70] and DPD[48] data, which argue that the direction of shifting the ODT curve depends on the copolymer composition, whereas lowering the critical point is rather weak if at all exists. Unfortunately, no experimental or MC modeling results are present in the literature for the case, when both blocks are highly polydisperse like in our simulations.

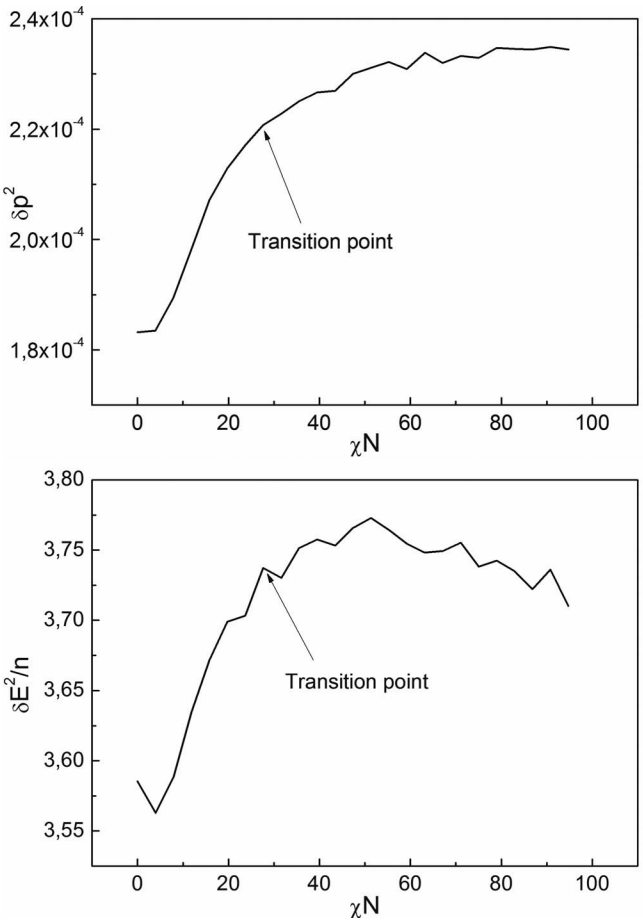

FIG. 9. Dependences of the (top) pressure and (bottom) internal energy variances on χN for the symmetric ($f = 0.5$) *r*-diblock.

Contrary to the monodisperse case, the ODT is not accompanied by a spike in fluctuations of the pressure and internal energy (Figure 9), which means that the transition is of the second or higher order, the same being related to the OOTs. Since the WM phase lacks long-range order, the D → WM transition can be detected only visually with relatively low accuracy, which is reflected by the high error bars in the phase diagram (Figure 8). Some difficulties are also met with locating the D → S transition since fine ordering of spheres requires considerably more time than the equilibration of other microstructures, not to mention that the morphological relaxation in random copolymers is much slower than in regular ones.

Moderate polydispersity of one block ($PDI_A = 1.3$, $PDI_B \approx 1$) was proved[71] to increase stability of the G phase through spatial redistribution of blocks leading to the relaxation of "packing frustrations" inherent in that phase. However, further increase in PDI_A up to 1.5 resulted in leveling the energies of the G and PL phases,[20] while at $PDI_A = 1.8$ the blend of AB diblocks with different compositions exhibited macrophase separation.[72] Our *r*-diblocks demonstrate similar tendencies at even higher polydispersity degrees ($PDI_A = PDI_B \approx 2$): depending on χN value, they can undergo the transition L → PL → C without forming a gyroid at all or L → PL → 3d/C → C including phase coexistence. Note that the possibility of polydispersity-driven macrophase

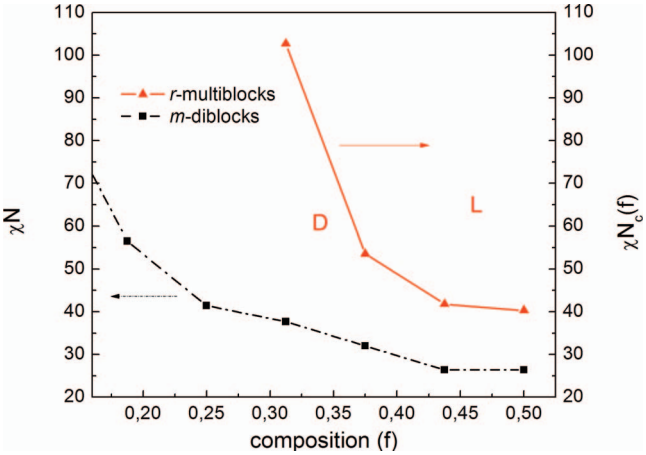

FIG. 10. ODT curves for *m*-diblocks and *r*-multiblocks.

separation in systems with a unimodal molecular mass distribution is still an open question.[45,68]

C. Random multiblocks

Calculations reveal that the phase diagram for *r*-multiblocks contains only D and L domains separated by the ODT curve, which is plotted in Figure 10 along with the corresponding ODT curve for *m*-diblocks. The ordinate is χN for diblocks, where $N = 16$, and χN_c for multiblocks, where the constituting length N_c is composition-dependent and given by Eq. (9) with $\bar{N} = 32$. The critical point for *r*-multiblocks is found at $(\chi N_c)_{cr} = 40.2$ so that for a symmetric copolymer with $N_c \approx 2$ (Eq. (9)) χ_{cr} should be as high as 20.1. Thus, fully random multiblock AB copolymers undergo microphase separation only in the case of very high incompatibility of A and B units, as was predicted by theory[73] and MC simulations.[74] In the compositionally asymmetric case, even higher values of χN_c are needed to attain the ODT and no other ordered structures can be formed except lamellas. Similarly to *r*-diblocks, the transition for *r*-multiblocks is higher than of the first order at any composition.

It is also instructive to compare the domain spacing of the lamellar structures, D, for three types of AB copolymers considered in this study (Figure 11). For *m*-diblocks, the ratio $D/N^{1/2}$ is almost independent of χN at $\chi N < 6$, as it should be in the absence of segregation.[75] At $\chi N \approx 10$, i.e., still below the transition point, $D/N^{1/2}$ starts to grow, which reflects beginning of A and B blocks separation that leads to a corresponding increase in the mean gyration radius of a chain R_g (Fig. 12). Simultaneously, the mean gyration radius of similar (A or B) blocks decreases until $\chi N \approx 20$, when the blocks are most compact. Qualitatively similar behavior was reported in Ref. 54, where *m*-diblocks were studied by MC simulations. Inset in Fig. 12 demonstrates that at $\chi N \approx 20$ the structure factor for *r*-diblocks already possesses a pronounced maximum. As can be seen in Figure 11, the dependence $D/N^{1/2}$ on (χN) is most steep near the ODT at $(\chi N)_{cr} \approx 26.4$, which is qualitatively consistent with the theoretical predictions of Ref. 76. At $\chi N \approx 50$ $D/N^{1/2}$ begins to scale as $(\chi N)^{\nu}$, $\nu = 0.185 \pm 0.020$, and this dependence holds at least up to $\chi N = 100$, being in good agreement with experiment,[77] theory,[50] and MC modeling[78] for the strong segregation regime. However, diblock copolymers with longer chains must be tested to verify these conclusions.

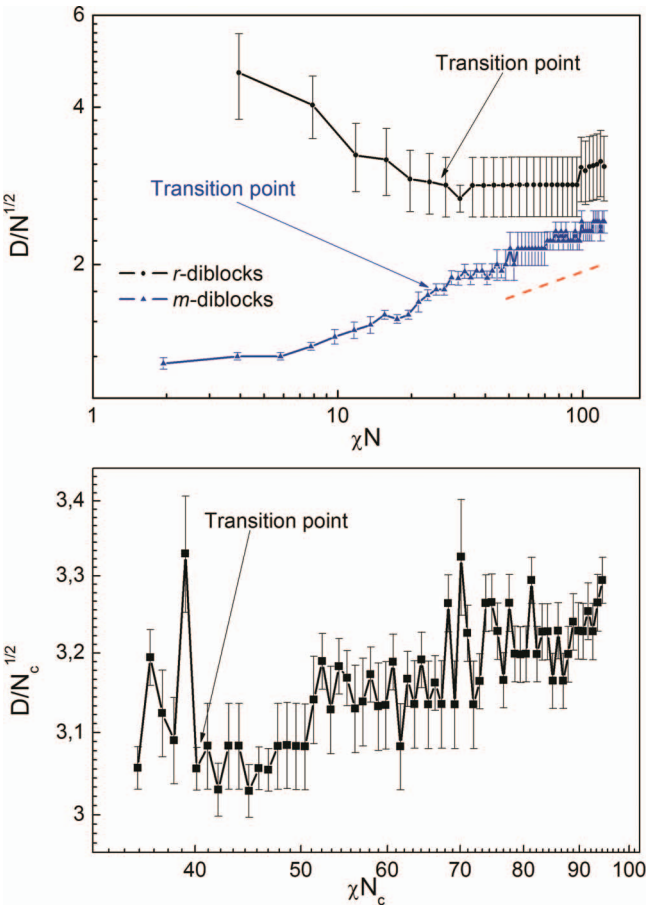

FIG. 11. Scaled domain spacing D for the symmetric (top) *m*- and *r*-diblocks and (bottom) *r*-multiblocks vs χN. SST prediction for *m*-diblocks is shown with the red dashed line.

The domain spacing in polydisperse *r*-diblocks appears to be considerably larger even in the disordered state,

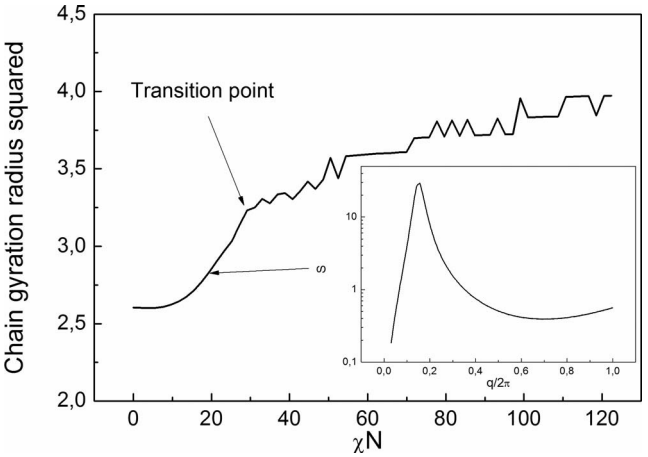

FIG. 12. Dependence of the mean chain gyration radius squared R_g^2 on χN for the symmetric *m*-diblocks. Typical static structure factor at $\chi N = 20$ is plotted in the inset.

presumably reflecting the segregation of the longest, most incompatible A and B blocks. With increasing χN, shorter blocks join the segregation process and the spacing decreases though it remains notably higher than in the corresponding *m*-diblocks, in agreement with the well established fact[45] that polydispersity in block copolymers increases the lamellar period. Surprisingly, we found that in the wide interval between $(\chi N)_{cr} \approx 27.6 < \chi N < 100$ the ratio $D/N^{1/2}$ does not depend on χN, which means that growing incompatibility of A and B units causes redistributions in the lamellas of polydisperse diblocks that completely relax chain stretching. Within that interval, the domain spacing ratio for *r*- and *m*-diblocks decreases with χN, which is consistent with SCFT calculations for high polydispersities.[49]

The domain spacing in *r*-multiblocks is a highly fluctuating quantity, which is almost independent on χN_c. However, blocks in symmetric fully random copolymers are extremely short, which explains a very restricted potential of lamellas to change their thickness.

V. CONCLUSIONS AND OUTLOOK

In this paper, we presented the state-of-the-art phase diagrams for three binary block copolymer melts, which were obtained using the DPD simulation technique on a modern computational cluster. As a coarse-grained molecular dynamics method, DPD naturally avoids difficulties of theoretical approaches (such as accounting for fluctuations and finite chain lengths) and Monte Carlo simulations (lattice effects and hard interaction potentials), though obtaining well-defined complex microstructures, such as the gyroid, still remains a weak point of the DPD technique.

The diagram for monodisperse diblocks reproduces all main domains of the SCFT diagram, which is the product of a number of theoretical studies, and demonstrates clear advantage over the MC diagram. It is shown that the mean square pressure fluctuation exhibits a spike in all order-disorder transition points, i.e., that the transition is of the first order, in contrast to ODTs in the other copolymers considered in this study and all order-order transitions, which are of higher order. The diagram for polydisperse diblocks contains new information, since only weak-segregation theory calculations[62–64] and no experimental data, up to our knowledge, were previously reported for the model, in which both blocks are characterized by the Flory distribution in length. Oppositely to the theoretical predictions, we find that polydispersity does not have much influence on the ODT curve. However, some of the phase domains are considerably shifted in comparison to the monodisperse case, for instance, the L and C domains are shrunk, the PL domain is enlarged, the pure 3d-bicontinuous phase (most probably, the gyroid) disappears, and the WM phase enters the diagram. A pronounced effect of polydispersity on the domain spacing in the L phase is found, which goes beyond casual lamella thickening. Contrary to the well known SST behavior for monodisperse diblocks, $D/N^{1/2} \sim (\chi N)^{1/6}$, which is successfully reproduced in our calculations, the scaled domain spacing for polydisperse diblocks, $D/N^{1/2}$, is nearly independent of χN from the transition point and up to $\chi N \approx 100$. As a result, the lamella thickness ratio for polydisperse and monodisperse diblocks decreases with χN in the mentioned wide interval. The diagram for completely random multiblocks contains only disordered and lamellar phases due to the extremely small length of the constituting blocks and even the L phase is formed only in the case of very high incompatibility of A and B units. It should be noted that experimental or obtained by computer simulations phase diagrams for such copolymers are absent in the literature.

Concerning possible future applications of DPD to studying the phase behavior of block copolymers we would like to mention, first of all, Markovian (random correlated) multiblock copolymers, a model that was deeply studied in theory since the seminal paper by Milner, Fredrickson, and Leibler[79] and recently attracted the attention of experimentalists[80–82] due to the progress in the controlled synthesis of multiblock polyolefins.[83] Comprehensive simulation techniques[84] reveal only short-range order in the disordered phase (microemulsion), which, however, possesses interesting mechanical characteristics, and it would be interesting to search for long-range ordered structures with the help of DPD.

Secondly, exploring with DPD can be practically useful for specifying conditions for experimental studies on the block copolymers of complex architecture. At the moment, the phase behavior of such systems can be investigated in the framework of SCFT[44] and DPD can appear a useful alternative or supplementary tool.

Being an intrinsically dynamic method, DPD allows one to study the evolution of block copolymer systems in the course of ODT and OOT phase transitions. Along this line, it would be interesting to compare the DPD predictions not only with the experimental data, as it was done in Ref. 39 but also with the results of numerical analysis by other particle- and field-based theoretical approaches. Such comparative study of DPD and Brownian dynamics, on the one side, and DPD and the dynamic version of SCFT,[85,86] on the other side, was initiated in the pioneering DPD studies[25,26] and it definitely worth continuing it at the modern level of computing facilities. However, we are unaware of phase diagrams for copolymer systems constructed using dynamical SCFT.

Finally, a lot of open problems are waiting for researchers who are interested in the role of polydispersity in block copolymer systems.[45] In this work, we studied only one system with the exponential distribution of both blocks, while synthetic methods are able to produce a diversity of molecular mass distributions so that the corresponding copolymers can be ordered in a completely different way than their monodisperse analogues.

ACKNOWLEDGMENTS

The authors thank Professor P. G. Khalatur and Professor M. Müller for fruitful discussions. One of the authors (A.A.G.) is grateful to Russian Foundation of Basic Research for the financial support (Grant No. 12-03-31252 mol_a). We thank Moscow State University Supercomputer Center for providing the computational resources.[87]

[1]F. S. Bates and G. H. Fredrickson, Phys. Today **52**(2), 32 (1999).
[2]V. Abetz and P. F. W. Simon, Adv. Polym. Sci. **189**, 125 (2005).

[3] A. J. Meuler, M. A. Hillmyer, and F. S. Bates, Macromolecules **42**, 7221 (2009).
[4] F. S. Bates, M. A. Hillmyer, T. P. Lodge, C. M. Bates, K. T. Delaney, and G. H. Fredrickson, Science **336**, 434 (2012).
[5] M. Müller and F. Schmid, Adv. Polym. Sci. **185**, 1 (2005).
[6] G. H. Fredrickson, *The Equilibrium Theory of Inhomogeneous Polymers* (Oxford University Press, New York, 2006).
[7] V. Ortiz, S. O. Nielsen, M. L. Klein, and D. E. Discher, J. Polym. Sci., Part B: Polym. Phys. **44**, 1907 (2006).
[8] K. Binder, M. Müller, and R. L. C. Vink, Macromol. Theory Simul. **20**, 600 (2011).
[9] E. Weinan, *Principles of Multiscale Modeling* (Cambridge University Press, 2011).
[10] G. Milano and T. Kawakatsu, J. Chem. Phys. **130**, 214106 (2009).
[11] D. Q. Pike, F. A. Detcheverry, M. Müller, and J. J. de Pablo, J. Chem. Phys. **131**, 084903 (2009).
[12] M. Müller, J. Stat. Phys. **145**, 967 (2011).
[13] P. Padmanabhan, F. J. Martinez-Veracoechea, J. C. Araque, and F. A. Escobedo, J. Chem. Phys. **136**, 234905 (2012).
[14] H. Guo and K. Kremer, J. Chem. Phys. **118**, 7714 (2003).
[15] C. Pierleoni, C. Addison, J. P. Hansen, and V. Krakoviack, Phys. Rev. Lett. **96**, 128302 (2006).
[16] F. Eurich, A. Karatchensev, J. Baschnagel, W. Dieterich, and P. Maass, J. Chem. Phys. **127**, 134905 (2007).
[17] C. Gross and W. Paul, Soft Matter **6**, 3273 (2010); Polym. Sci., Ser. C **55**, 94 (2013).
[18] A. D. Litmanovich, V. V. Podbelskiy, and Y. V. Kudryavtsev, Macromol. Theory Simul. **19**, 269 (2010).
[19] T. M. Beardsley and M. W. Matsen, Eur. Phys. J. E **32**, 255 (2010).
[20] T. M. Beardsley and M. W. Matsen, Macromolecules **44**, 6209 (2011).
[21] J. R. Spaeth, I. G. Kevrekidis, and A. Z. Panagiotopoulos, J. Chem. Phys. **134**, 164902 (2011).
[22] J. R. Spaeth, T. Dale, I. G. Kevrekidis, and A. Z. Panagiotopoulos, Ind. Eng. Chem. Res. **50**, 69 (2011).
[23] P. Espanol and P. B. Warren, Europhys. Lett. **30**, 191 (1995).
[24] R. D. Groot and P. B. Warren, J. Chem. Phys. **107**, 4423 (1997).
[25] R. D. Groot and T. J. Madden, J. Chem. Phys. **108**, 8713 (1998).
[26] R. D. Groot, T. J. Madden, and D. J. Tildesley, J. Chem. Phys. **110**, 9739 (1999).
[27] L.-J. Chen, Z.-Y. Lu, H. J. Qian, Z.-S. Li, and C.-C. Sun, J. Chem. Phys. **122**, 104907 (2005).
[28] F. J. Martinez-Veracoechea and F. A. Escobedo, J. Chem. Phys. **125**, 104907 (2006).
[29] A. R. Khokhlov and P. G. Khalatur, Chem. Phys. Lett. **461**, 58 (2008).
[30] X. Li, I. V. Pivkin, H. Liang, and G. E. Karniadakis, Macromolecules **42**, 3195 (2009).
[31] H. Chen and E. Ruckenstein, Soft Matter **8**, 1327 (2012).
[32] T. Klymko, V. Markov, A. Subbotin, and G. ten Brinke, Soft Matter **5**, 98 (2009).
[33] C.-I. Huang, C.-H. Liao, and T. P. Lodge, Soft Matter **7**, 5638 (2011).
[34] A. A. Gavrilov, Y. V. Kudryavtsev, P. G. Khalatur, and A. V. Chertovich, Chem. Phys. Lett. **503**, 277 (2011).
[35] Y. L. Wang, B. Li, Y. F. Zhou, Z. Y. Lu, and D. Y. Yan, Soft Matter **9**, 3293 (2013).
[36] H.-J. Qian, Z.-Y. Lu, L.-J. Chen, Z.-S. Li, and C.-C. Sun, Macromolecules **38**, 1395 (2005).
[37] W.-J. Lee, S.-P. Ju, Y.-C. Wang, and J.-G. Chang, J. Chem. Phys. **127**, 064902 (2007).
[38] V. Ortiz, S. O. Nielsen, D. E. Discher, M. L. Klein, R. Lipowsky, and J. Shillcock, J. Phys. Chem. B **109**, 17708 (2005).
[39] C. Soto-Figueroa, M.-R. Rodriguez-Hidalgo, J.-M. Martinez-Magadan, and L. Vicente, Macromolecules **41**, 3297 (2008).
[40] S. Roy, D. Markova, A. Kumar, M. Klapper, and F. Müller-Plathe, Macromolecules **42**, 841 (2009).
[41] X. Li, J. Guo, Y. Liu, and H. Liang, J. Chem. Phys. **130**, 074908 (2009).
[42] H. Tan, Z. Wang, J. Li, Z. Pan, M. Ding, and Q. Fu, ACS Macro Lett. **2**, 146 (2013).
[43] A. Vazquez-Quesada, M. Ellero, and P. Espanol, J. Chem. Phys. **130**, 034901 (2009).
[44] M. W. Matsen, Macromolecules **45**, 2161 (2012).
[45] N. A. Lynd, A. J. Meuler, and M. A. Hillmyer, Prog. Polym. Sci. **33**, 875 (2008).
[46] D. V. Guseva, Y. V. Kudryavtsev, and A. V. Berezkin, J. Chem. Phys. **135**, 204904 (2011).
[47] A. A. Gavrilov, D. V. Guseva, Y. V. Kudryavtsev, P. G. Khalatur, and A. V. Chertovich, Polym. Sci., Ser. A **53**, 1207 (2011).
[48] Y. Li, H.-J. Qian, and Z.-Y. Lu, Polymer **54**, 3716 (2013).
[49] M. W. Matsen, Eur. Phys. J. E **21**, 199 (2006).
[50] A. N. Semenov, Sov. Phys. JETP **61**, 733 (1985).
[51] I. A. Nyrkova, A. R. Khokhlov, and M. Doi, Macromolecules **26**, 3601 (1993).
[52] G. Besold, I. Vattulainen, M. Karttunen, and J. M. Polson, Phys. Rev. E **62**, R7611 (2000).
[53] M. P. Allen and D. J. Tildesley, *Computer Simulation of Liquids* (Clarendon Press, Oxford, 1987).
[54] O. N. Vassiliev and M. W. Matsen, J. Chem. Phys. **118**, 7700 (2003).
[55] M. W. Matsen and M. Schick, Phys. Rev. Lett. **72**, 2660 (1994).
[56] Y. Liu, J. D. Spring, M. Steinhart, and R. Bansil, Macromolecules **45**, 9147 (2012).
[57] N. Sota, K. Saijo, H. Hasegawa, T. Hashimoto, Y. Amemiya, and K. Ito, Macromolecules **46**, 2298 (2013).
[58] P. V. Komarov, I. N. Veselov, P. P. Chu, P. G. Khalatur, and A. R. Khokhlov, Chem. Phys. Lett. **487**, 291 (2010).
[59] M. I. Kim, T. Wakada, S. Akasaka, S. Nishitsuji, K. Saijo, H. Hasegawa, K. Ito, and M. Takenaka, Macromolecules **42**, 5266 (2009).
[60] C. D. Han, N. Y. Vaidya, D. Kim, G. Shin, D. Yamaguchi, and T. Hashimoto, Macromolecules **33**, 3767 (2000).
[61] L. Leibler, Macromolecules **13**, 1602 (1980).
[62] G. H. Fredrickson and E. Helfand, J. Chem. Phys. **87**, 697 (1987).
[63] L. Leibler and H. Benoit, Polymer **22**, 195 (1981).
[64] K. M. Hong and J. Noolandi, Polym. Commun. **25**, 265 (1984).
[65] C. Burger, W. Ruland, and A. N. Semenov, Macromolecules **23**, 3339 (1990); **24**, 816 (1991).
[66] S. W. Sides and G. H. Fredrickson, J. Chem. Phys. **121**, 4974 (2004).
[67] D. M. Cooke and A.-C. Shi, Macromolecules **39**, 6661 (2006).
[68] M. W. Matsen, Phys. Rev. Lett. **99**, 148304 (2007).
[69] N. A. Lynd and M. A. Hillmyer, Macromolecules **40**, 8050 (2007).
[70] T. M. Beardsley and M. W. Matsen, Eur. Phys. J. E **27**, 323 (2008).
[71] A. J. Meuler, C. J. Ellison, M. A. Hillmyer, and F. S. Bates, Macromolecules **41**, 6272 (2008).
[72] Y. Matsushita, A. Noro, M. Iinuma, J. Suzuki, H. Ohtani, and A. Takano, Macromolecules **36**, 8074 (2003).
[73] E. I. Shakhnovich and A. M. Gutin, J. Phys. (France) **50**, 1843 (1989).
[74] B. W. Swift and M. Olvera de la Cruz, Europhys. Lett. **35**, 487 (1996).
[75] K. R. Shull, Macromolecules **25**, 2122 (1992).
[76] M. W. Matsen and F. S. Bates, Macromolecules **29**, 1091 (1996).
[77] H. Hasegawa, H. Tanaka, K. Yamasaki, and T. Hashimoto, Macromolecules **20**, 1651 (1987).
[78] M. Murat, G. S. Grest, and K. Kremer, Macromolecules **32**, 595 (1999).
[79] G. H. Fredrickson, S. T. Milner, and L. Leibler, Macromolecules **25**, 6341 (1992).
[80] S. Li, R. Register, J. D. Weinhold, and B. G. Landes, Macromolecules **45**, 5773 (2012).
[81] G. M. Liu, Y. Guan, T. Wen, X. W. Wang, X. Q. Zhang, D. J. Wang, X. H. Li, J. Loos, H. Y. Chen, K. Walton, and G. Marchand, Polymer **52**, 5221 (2011).
[82] J. Jin, J. A. Du, Q. H. Xia, Y. R. Liang, and C. C. Han, Macromolecules **43**, 10554 (2010).
[83] P. S. Chum and K. W. Swogger, Prog. Polym. Sci. **33**, 797 (2008).
[84] B. Steinmüller, M. Müller, K. R. Hambrecht, G. D. Smith, and D. Bedrov, Macromolecules **45**, 1107 (2012).
[85] N. M. Maurits and J. G. E. M. Fraaije, J. Chem. Phys. **107**, 5879 (1997).
[86] B. A. C. van Vlimmeren, N. M. Maurits, A. V. Zvelindovsky, G. J. A. Sevink, and J. G. T. M. Fraaije, Macromolecules **32**, 646 (1999).
[87] See http://hpc.msu.ru/ for the information about the supercomputers "Lomonosov" and "Chebyshev" used in our study.